Applied Catalysis B: Environmental 111–112 (2012) 326–333

Contents lists available at SciVerse ScienceDirect

Applied Catalysis B: Environmental

journal homepage: www.elsevier.com/locate/apcatb

Enhanced visible-light photocatalytic activity of Bi_2WO_6 nanoparticles by Ag_2O cocatalyst

Huogen Yu[a,c,*], Rui Liu[a], Xuefei Wang[a,c], Ping Wang[a,c], Jiaguo Yu[b,**]

[a] Department of Chemistry, School of Science, Wuhan University of Technology, Wuhan 430070, People's Republic of China
[b] State Key Laboratory of Advanced Technology for Material Synthesis and Processing, Wuhan University of Technology, Wuhan 430070, People's Republic of China
[c] Institute of High Pressure and Temperature Physics, School of Science, Wuhan University of Technology, Wuhan 430070, People's Republic of China

ARTICLE INFO

Article history:
Received 27 July 2011
Received in revised form 6 October 2011
Accepted 10 October 2011
Available online 17 October 2011

Keywords:
Cocatalyst
$Ag–Ag_2O$
Photocatalysis
Bi_2WO_6
Visible light

ABSTRACT

Cocatalyst modification is an efficient strategy to improve the photocatalytic efficiency of photocatalysts by promoting the effective separation of photogenerated electrons and holes. However, most of the cocatalysts are restricted to noble metals (e.g., Ag, Au, Pt) and seldom investigation has been focused on their oxides. In this study, Ag_2O cocatalyst was coated on the surface of Bi_2WO_6 nanoparticles by an impregnation method followed by a low-temperature treatment (100–350 °C) and their photocatalytic performance was evaluated by the photocatalytic decolorization of methyl orange solution under visible-light irradiation. It was found that after the surface coating of Ag_2O, the obtained Ag_2O/Bi_2WO_6 composites exhibited an obvious higher photocatalytic activity than the unmodified Bi_2WO_6 nanoparticles and N-doped TiO_2. Owing to the photosensitive property of pure Ag_2O phase, the $Ag–Ag_2O$ composite easily formed during the decomposition process of organic substances under visible-light irradiation. On the bases of experimental result and band structure analysis, an $Ag–Ag_2O$ cocatalyst-enhanced photocatalytic mechanism is proposed; namely, the $Ag–Ag_2O$ cocatalyst possibly reduces oxygen via a multi-electron transfer mechanism. The present results suggest that $Ag–Ag_2O$ can act as a new and effective cocatalyst for the enhanced photocatalytic performance of photocatalysts, which provides a new approach for the design and development of high-performance visible-light photocatalysts.

1. Introduction

Heterogeneous photocatalysis has been considered as a cost-effective alternative for the environmental applications in air purification, water disinfection, and hazardous water remediation [1–5]. Despite its great potential, the fast recombination rate of photogenerated electron–hole pairs on the surface or in the lattice of a photocatalyst hinders the commercialization of photocatalytic oxidation technology [6–8]. To improve photocatalytic efficiency, one of the effective strategies is to develop cocatalyst-modified photocatalysts such as Au/TiO_2 [9–12] and Ag/TiO_2 [13–15]. The general principle for the enhanced photocatalytic performance is that the formation of a space-charge layer at the cocatalyst–semiconductor interface improves the charge-separation rate after band-gap excitation [16,17]. However, the previous studies about the cocatalyst–semiconductor composites were mainly focused on the development of various semiconductor photocatalytic materials, while less investigations about the cocatalysts have been concerned.

Since heterogeneous photocatalytic reactions usually take place on the surface of a photocatalyst and cocatalyst functions as a reduction or oxidation active site to promote the separation of photo-generated electrons and holes, the species and property of the cocatalyst play a very important role in determining photocatalytic efficiency. It is generally accepted that noble-metal nanoparticle (such as Au, Ag and Pt) usually functions as an electron sink to accept photogenerated electrons from excited semiconductor and then acts as a reduction active site to reduction oxygen [18]. By loading noble-metal nanoparticles, Kamat et al. [19,20] found that there was a 3–5-fold improvement in the photoelectrochemical performance of the nanostructured TiO_2 films. Abe et al. [21] also reported the enhanced photocatalytic activity of WO_3 by loading Pt cocatalyst for the decomposition of acetaldehyde under visible-light irradiation. However, most of the present investigations about the cocatalysts are restricted to noble metals (e.g., Pt, Ag, Au), and seldom studies about their oxides have been explored [19–22].

More recently, we reported that the some transition metal ions such as Fe(III) and Cu(II) (or their oxides) could be work as efficient cocatalysts for the complete decomposition of 2-propanol into

* Corresponding author at: Department of Chemistry, School of Science, Wuhan University of Technology, Wuhan 430070, People's Republic of China.
Tel.: +86 27 87871029; fax: +86 27 87879468.
** Corresponding author. Tel.: +86 27 87871029; fax: +86 27 87879468.
E-mail addresses: yuhuogen@yahoo.cn (H. Yu), jiaguoyu@yahoo.com (J. Yu).

0926-3373/$ – see front matter © 2011 Elsevier B.V. All rights reserved.
doi:10.1016/j.apcatb.2011.10.015

CO_2 [23–25]. In this study, Ag_2O as a new cocatalyst was coated on the surface of Bi_2WO_6 nanoparticles to synthesize Ag_2O-modified Bi_2WO_6 (referred to as Ag_2O/Bi_2WO_6) nanoparticles and the photocatalytic performance of the Ag_2O/Bi_2WO_6 nanoparticles was evaluated by the photocatalytic decolorization of methyl orange solution under visible-light irradiation. A possible mechanism of Ag–Ag_2O as an efficient cocatalyst was proposed to account for the enhanced photocatalytic performance of Bi_2WO_6 nanoparticles. To the best of our knowledge, this is the first report about the Ag–Ag_2O working as an active cocatalyst to increase the photocatalytic activity of semiconductor. This work may provide new insights for the design and preparation of new high-efficiency visible-light photocatalysts.

2. Experimental

2.1. Preparation of Bi_2WO_6 nanoparticles

All the reagents were of analytical grade and were used without any further purification. Bi_2WO_6 nanoparticles were synthesized by a facile participation reaction. In a typical synthesis procedure, 11.15 g of $Bi(NO_3)_3{\cdot}5H_2O$ and 3.80 g of $Na_2WO_4{\cdot}2H_2O$ were firstly dissolved in 50 mL of distilled water, respectively. A precipitation was obtained when the two solutions were mixed together under magnetic stirring at room temperature for 60 min. After filtered, washed with distilled water and then dried at 80 °C for 2 h, the resulting power was calcined at 500 °C for 2 h.

2.2. Preparation of Ag_2O-modified Bi_2WO_6 nanoparticles

Ag_2O-modified Bi_2WO_6 (Ag_2O/Bi_2WO_6) nanoparticles were prepared by an impregnation method. Briefly, 1.00 g of Bi_2WO_6 nanoparticles was dispersed in a 9.26 mL of $AgNO_3$ solution (0.10 mol/L) to form a suspension (Ag/Bi_2WO_6 = 10 wt%). After stirring for 2 h, the resulting suspension was dried at 60 °C and was then calcined at 100, 200 and 350 °C for 30 min, respectively. The resulting sample was ground into a fine powder to obtain the Ag_2O/Bi_2WO_6 nanoparticles. As the low-temperature calcination (<400 °C) was performed for the preparation of Ag_2O/Bi_2WO_6 composites, the Ag_2O phase may exists only on the surface of Bi_2WO_6 nanoparticles and would not be doped into the lattices. In addition, Ag/Bi_2WO_6 composite sample was also prepared by a high-temperature calcination of Ag_2O/Bi_2WO_6 at 450 °C owing to the decomposition of Ag_2O to metallic Ag [26].

To investigate the effect of Ag_2O amount on the photocatalytic performance of Bi_2WO_6 nanoparticles, the Ag_2O/Bi_2WO_6 nanoparticles with different amount of Ag_2O (Ag/Bi_2WO_6 = 1–30 wt%) were prepared at 350 °C. For comparison, the Ag_2O was also coated on the surface of Al_2O_3 particles (referred to as Ag_2O/Al_2O_3) under the identical experimental conditions and was then calcined at 350 °C for 30 min.

2.3. Preparation of N-doped TiO_2

The preparation of N-doped TiO_2 ($TiO_{2-x}N_x$) was also described in our previous study [27]. Briefly, 17 mL of tetrabutylorthotitanate was added into an $NH_3{\cdot}H_2O$ solution (NH_3 = 0–10 wt%) under stirring. After stirring for 1 h, the suspension solution was aged at room temperature (25 °C) for 24 h. The resulted suspension was filtrated, washed with distilled water and dried at 60 °C for 6 h, and then was calcined at 500 °C for 2 h to obtain $TiO_{2-x}N_x$. It was found that when the concentration of NH_3 was controlled to be 1 wt%, the obtained $TiO_{2-x}N_x$ showed the highest photocatalytic activity. Thus, the $TiO_{2-x}N_x$ prepared from the 1 wt% of NH_3 solution was used as the reference in this study. The obtained $TiO_{2-x}N_x$ sample was anatase phase according to XRD results and the x was 0.019 based on the XPS analysis. The specific surface area and pore volume of the $TiO_{2-x}N_x$ sample were 55.4 m^2/g and 0.19 cm^3/g, respectively.

2.4. Characterization

X-ray diffraction (XRD) patterns were obtained on a Rigaku Ultima III X-ray Diffractometer (Japan) using Cu Kα radiation. Morphological analysis was performed by an S-4800 field-emission scanning electron microscope (FE-SEM, Hitachi, Japan) with an acceleration voltage of 10 kV. UV–vis absorption spectra were obtained using a UV–visible spectrophotometer (UV-2550, SHIMADZU, Japan). Transmission electron microscopy (TEM) analyses were conducted by a JEM-2100F electron microscope (JEOL, Japan) using a 200 kV accelerating voltage. X-ray photoelectron spectroscopy (XPS) measurements were done on a KRATOA XSAM800 XPS system with Mg Kα source. All the binding energies were referenced to the C 1s peak at 284.8 eV of the surface adventitious carbon. Nitrogen adsorption–desorption isotherms were obtained on an ASAP 2020 (Micromeritics Instruments, USA) nitrogen adsorption apparatus. The sample was degassed at 60 °C prior to BET measurements. The Brunauer–Emmett–Teller (BET) specific surface area (S_{BET}) was determined by a multipoint BET method using the adsorption data in the relative pressure (P/P_0) range of 0.05–0.25.

2.5. Photocatalytic activity

The evaluation of photocatalytic activity of the prepared samples for the photocatalytic decolorization of methyl orange (MO) aqueous solution was performed at ambient temperature. Experimental details were shown as follows: 0.05 g of the sample was dispersed into 10 mL of MO solution (20 mg/L) in a disk with a diameter of ca. 5 cm. The solution was allowed to reach an adsorption–desorption equilibrium among the photocatalyst, MO, and water before visible-light irradiation. A 350 W xenon lamp equipped with a UV-cutoff filter (providing visible light with $\lambda \geq 400$ nm) was used as a visible-light source. The average light intensity striking the surface of the reaction solution was about 80 mW cm^2. The concentration of MO was determined by an UV–visible spectrophotometer (UV-2550, SHIMADZU, Japan). After visible-light irradiation for some time, the reaction solution was centrifuged to measure the concentration of MO. As for the methyl orange aqueous solution with low concentration, its photocatalytic decolorization is a pseudo-first-order reaction and its kinetics may be expressed as $\ln(c_0/c) = kt$, where k is the apparent rate constant, and c_0 and c are the methyl orange concentrations at initial state and after irradiation for t min, respectively [28,29]. In addition, the colorless phenol (10 mg/L) and p-chlorophenol (13 mg/L) were also used as the target organic substances to evaluate the photocatalytic performance of the obtained samples under visible-light irradiation.

3. Results and discussion

3.1. Morphology and phase structures

Fig. 1 shows the SEM images of the Bi_2WO_6 nanoparticles before and after surface modification by Ag_2O cocatalyst. The size of the as-prepared Bi_2WO_6 nanoparticles is in the range of 30–100 nm (Fig. 1a). After surface modification by Ag_2O at 350 °C, the particle size of the Bi_2WO_6 has no obvious increase due to the high-temperature (500 °C) pre-treatment of Bi_2WO_6 precursor (Fig. 1b).

Fig. 2A shows the XRD patterns of the Ag_2O/Bi_2WO_6 nanoparticles calcined at various temperatures. It is found that all the diffraction peaks can be attributed to the orthorhombic Bi_2WO_6

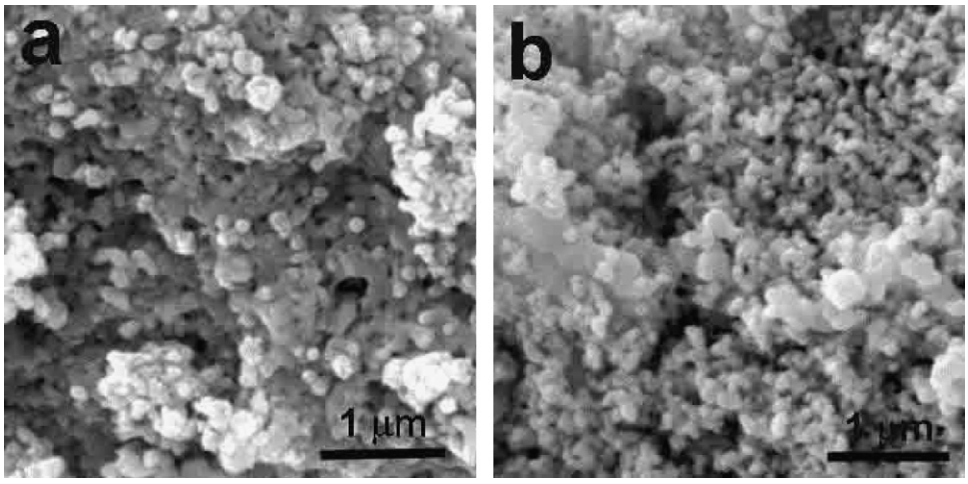

Fig. 1. SEM images of (a) Bi_2WO_6 nanoparticles and (b) Ag_2O/Bi_2WO_6 composite nanoparticles (350 °C).

(JCPDS no. 39-0256) in addition to a small amount of $Bi_{14}W_2O_{27}$ [30], while no diffraction peaks about Ag_2O and Ag phases can be found. In order to further demonstrate the phase structures of Ag element on the surface of Bi_2WO_6 nanoparticles, the characteristic diffraction peak of Ag_2O at ca. 38.3° (JCPDS no. 41-1104) and metallic Ag at ca. 44.3° (JCPDS no. 04-0783) were further measured, and the corresponding results are shown in Fig. 2B and C, respectively. Compared with the precursor Bi_2WO_6 nanoparticles, a weak diffraction peak (Fig. 2B, curve b and c) of Ag_2O can be observed after calcination at 200 °C and 350 °C, while metallic Ag begins to produce when the calcination temperature increases to 450 °C (Fig. 2C, curve d) due to the decomposition of Ag_2O [26]. The above results suggest that the Ag_2O phase can be successfully coated on the surface of Bi_2WO_6 nanoparticles by controlling the calcination temperature (<350 °C).

The phase structure of Ag_2O on the surface of Bi_2WO_6 nanoparticles can be further demonstrated by TEM analysis, as shown in Fig. 3. The Ag_2O modification has no obvious effect on the size of Bi_2WO_6 nanoparticles (30–100 nm) (Fig. 3a), in good agreement with the SEM results. High-magnification TEM image (Fig. 3b) of Ag_2O/Bi_2WO_6 nanoparticles indicates that the Ag_2O phase cannot be clearly found on the surface of Bi_2WO_6 nanoparticles. In view of a weak diffraction peak of Ag_2O in Fig. 2B, it can be deduced that the Ag_2O cocatalyst is mainly in poorly crystalline on the surface of Bi_2WO_6 nanoparticles. This can be further confirmed by the following experiments. When the high-energy-electron beam in the TEM system is striking on the surface of the Ag_2O/Bi_2WO_6 nanoparticle, metallic Ag nanoparticles with multiangular shape are gradually formed with increasing irradiation time (Fig. 3c) due to the decomposition of Ag_2O under the irradiation of

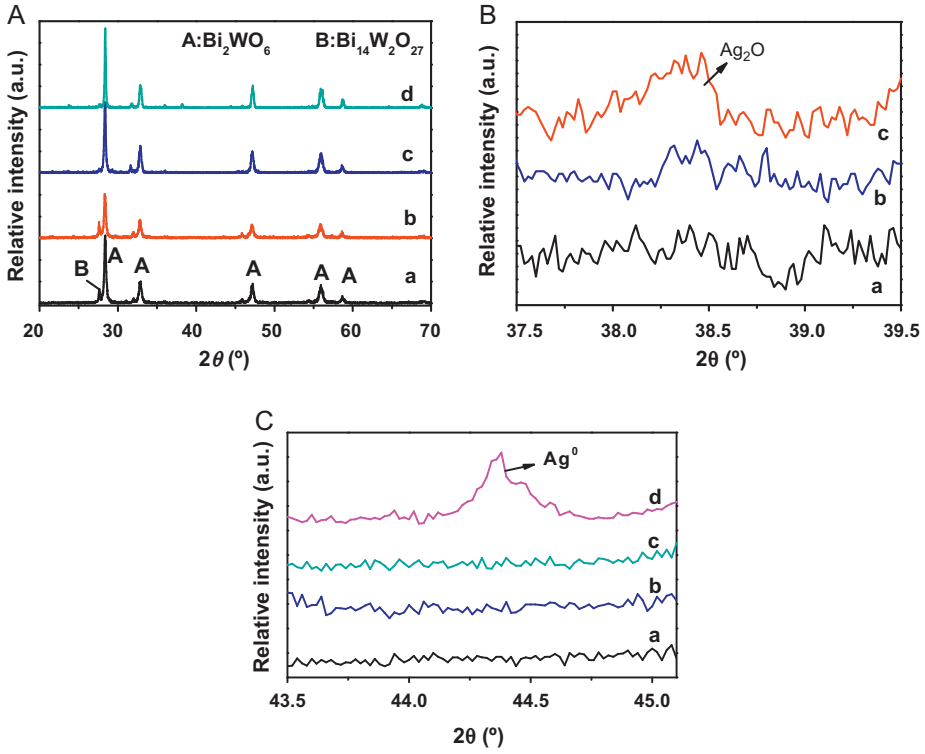

Fig. 2. Wide-angle XRD patterns (A) and their corresponding characterized diffraction peak of (B) Ag_2O and (C) metallic Ag phases: (a) Bi_2WO_6, (b) Ag_2O/Bi_2WO_6 composite nanoparticles (200 °C), (c) Ag_2O/Bi_2WO_6 composite nanoparticles (350 °C), and (d) Ag/Bi_2WO_6 composite nanoparticles (450 °C).

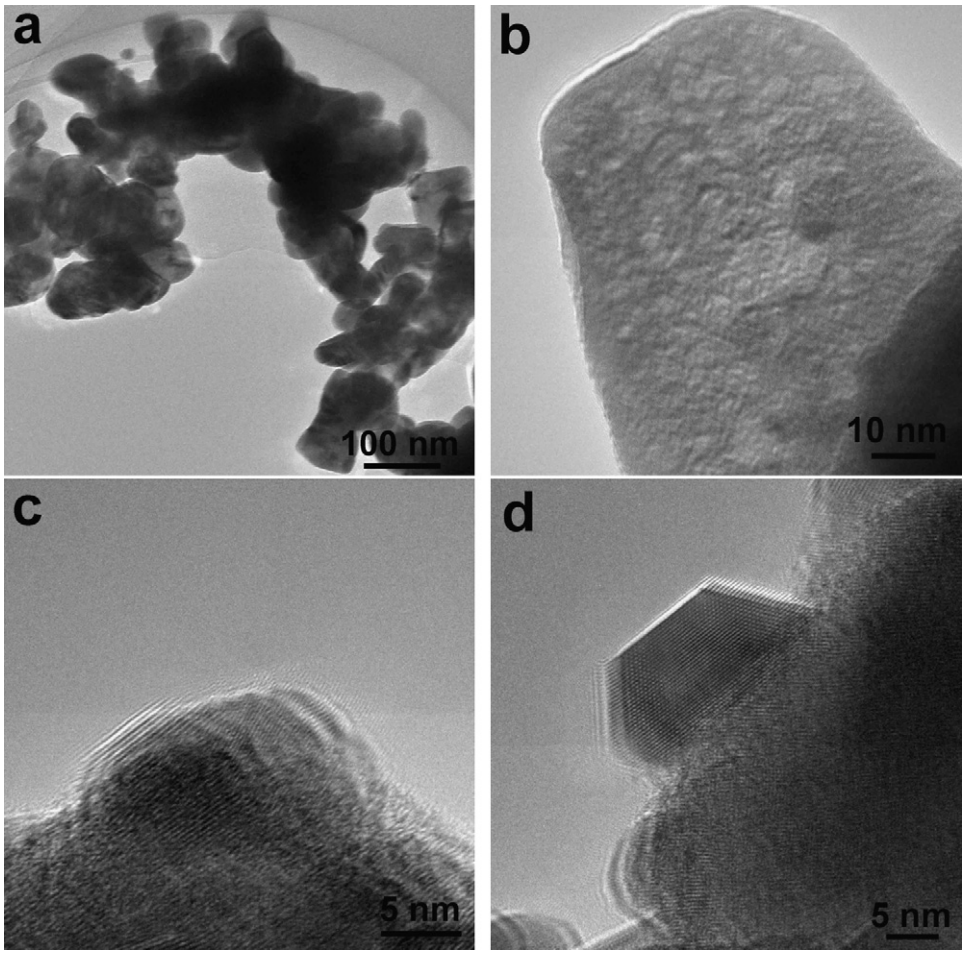

Fig. 3. TEM images of (a, b) the Ag_2O/Bi_2WO_6 composite nanoparticles (350 °C), (c) sample (b) after irradiation by electron beam in the TEM system, and (d) Ag/Bi_2WO_6 composite nanoparticles (450 °C).

high-energy-electron beam. In addition, when the Ag_2O/Bi_2WO_6 nanoparticles are calcined at 450 °C, some Ag nanoparticles can also be observed due to the decomposition of Ag_2O (Fig. 3d). The above results further strongly demonstrate that the Ag_2O on the surface of Bi_2WO_6 is a poorly crystalline phase, in good agreement with the XRD result.

3.2. UV–vis analysis

The phase structures and chemical states of Ag_2O on the surface of Bi_2WO_6 nanoparticles can be further characterized by UV–vis spectra, as shown in Fig. 4. As for the Bi_2WO_6 nanoparticles (Fig. 4a), only the band-gap absorption with an absorption edge at ca. 450 nm can be observed. After the surface of Bi_2WO_6 nanoparticles is coated with Ag_2O, the obtained Ag_2O/Bi_2WO_6 composite samples (Fig. 4b and c) exhibit a wide visible-light absorption in the range of 400–800 nm in addition to the band-gap absorption of Bi_2WO_6. With increasing calcination temperature to 450 °C, the visible-light absorption of the composite structures has an obvious increase due to the formation of metallic Ag nanoparticles (Fig. 4d). To further characterize the phase structures of the Ag element on the surface of Bi_2WO_6 nanoparticles, their difference UV–vis spectra are shown in the inset of Fig. 4. It is clear that no obvious absorption shoulder can be found for the low-temperature modified Bi_2WO_6 nanoparticles (≤350 °C). Since UV–vis spectrum is a very sensitive technology to detect the existing of noble metal nanoparticles due to their localized surface plasmon resonance in the visible-light region [27], the absence of plasmon absorption peak of metallic Ag nanoparticles in the range of 450–800 nm further demonstrates that the only possible specie of Ag element in the low-temperature modified Bi_2WO_6 nanoparticles (≤350 °C) is Ag_2O phase. As for the high-temperature modified Ag_2O/Bi_2WO_6 nanoparticles (450 °C), there is an obvious absorption peak (ca. 560 nm) with a wide range of 450–800 nm, which can be attributed to the formation of Ag nanoparticles (Fig. 2C, curve d) after the decomposition of Ag_2O [26]. The present results about UV–vis spectra are in good agreement with the XRD and TEM analysis.

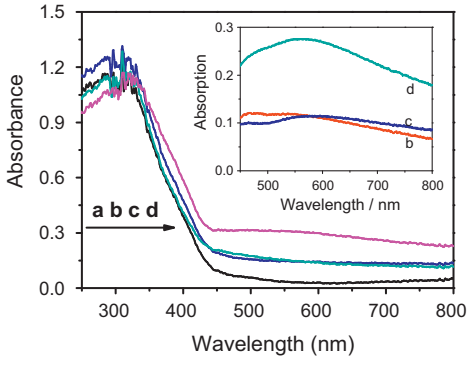

Fig. 4. UV–vis spectra of (a) Bi_2WO_6, (b) Ag_2O/Bi_2WO_6 composite nanoparticles (200 °C), (c) Ag_2O/Bi_2WO_6 composite nanoparticles (350 °C), and (d) Ag/Bi_2WO_6 composite nanoparticles (450 °C). The inset shows their corresponding difference UV–vis spectra.

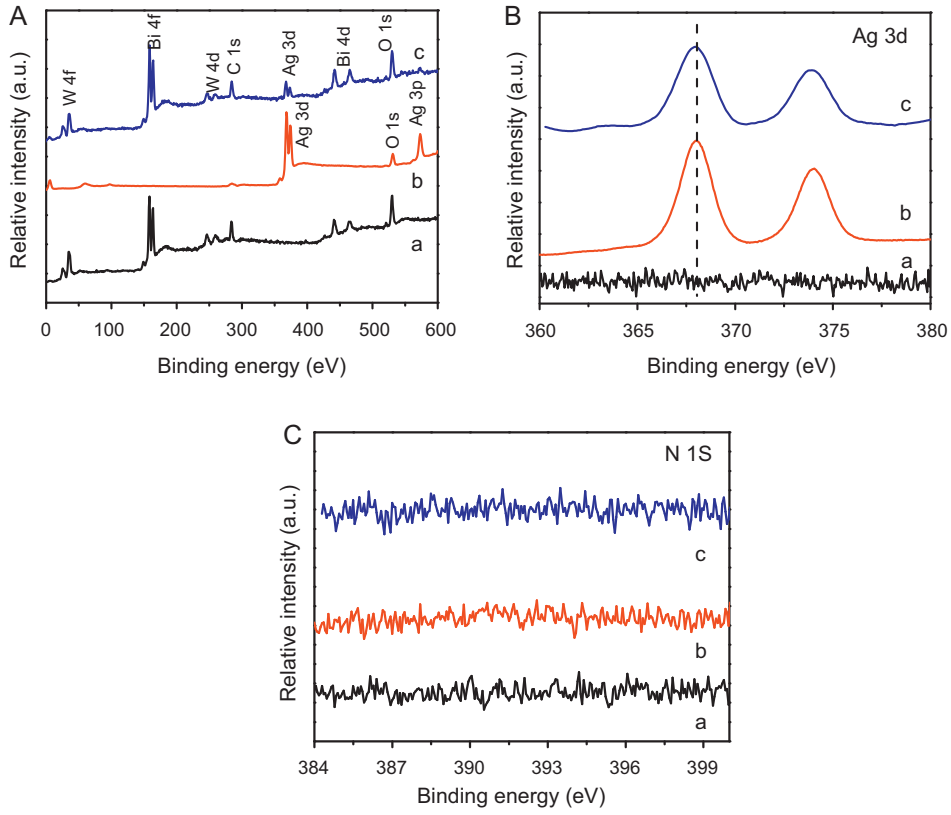

Fig. 5. XPS survey spectra (A), XPS spectra of Ag 3d (B) and N 1s (C) for the (a) Bi_2WO_6 nanoparticles, (b) Ag_2O, and (c) Ag_2O/Bi_2WO_6 composite nanoparticles (350 °C).

3.3. XPS analysis

The elemental composition of the Ag_2O/Bi_2WO_6 composite nanoparticles was analyzed by XPS. For comparison, pure Ag_2O powder, which was prepared by a precipitation reaction between $AgNO_3$ and NaOH solution under a dark condition, was also test by XPS. Compared with the precursor Bi_2WO_6 nanoparticles, a new Ag element is found in the Ag_2O/Bi_2WO_6 composite nanoparticles in addition to the Bi, W, O and C elements (Fig. 5A). The XPS peak for C 1s is due to the adventitious hydrocarbon from the XPS instrument itself. The Bi and W peaks are from the precursor Bi_2WO_6 nanoparticles, while the O element is from both the Bi_2WO_6 nanoparticles and Ag_2O cocatalyst. To further investigate the chemical states of Ag element, the high-resolution XPS peaks of Ag element are provided in Fig. 5B. The Ag_2O phase show XPS peaks with two individual peaks at ca. 368 eV and 374 eV (Fig. 5B, curve b), which can be assigned to Ag 3d5/2 and Ag 3d3/2 peaks in Ag_2O phase, respectively [31–33]. As for the Ag_2O/Bi_2WO_6 composite nanoparticles, the sample shows similar XPS peaks of Ag element with Ag_2O phase, indicating the formation of Ag_2O on the surface of Bi_2WO_6 nanoparticles, which is in good agreement with the XRD, TEM, and UV–vis results. In addition, no XPS peak of N 1s can be found (Fig. 5C), suggesting the effective removal of the NO_3^- in the precursor $AgNO_3$ during the preparation and low-temperature calcination processes. Therefore, the different microstructures and photocatalytic performance (see below) of Bi_2WO_6 nanoparticles and Ag_2O/Bi_2WO_6 composites are only caused by the loading of Ag_2O phase.

3.4. BET surface area and pore volume

The specific surface area and pore volume of the Ag_2O/Bi_2WO_6 composite nanoparticles were investigated by nitrogen adsorption–desorption isotherms. It was found that all the Bi_2WO_6 nanoparticles before and after modification by Ag_2O show a similar adsorption–desorption isotherms (not shown here), indicating a similar morphology and pore structure, as shown in Table 1. A typical nitrogen adsorption–desorption isotherm of the Ag_2O/Bi_2WO_6 composite nanoparticles after calcination at 350 °C is shown in Fig. 6. It is clear that the obtained Ag_2O/Bi_2WO_6 sample

Table 1
BET specific surface area (S_{BET}) and pore parameters of the Bi_2WO_6 and Ag_2O/Bi_2WO_6 nanoparticles prepared at various temperatures.

Samples	S_{BET} (m^2/g)	Pore volume (cm^3/g)	Pore size (nm)
Bi_2WO_6	7.2	0.012	6.2
100 °C	6.0	0.012	8.2
200 °C	6.3	0.017	10.9
350 °C	6.0	0.010	11.6
450 °C	5.9	0.008	8.0

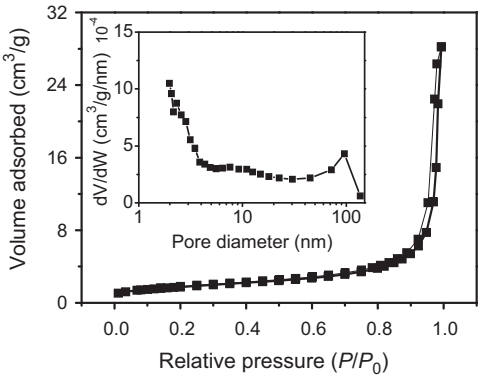

Fig. 6. Nitrogen adsorption–desorption isotherm and corresponding pore size distribution (inset) of the Ag_2O/Bi_2WO_6 composite nanoparticles obtained from 350 °C.

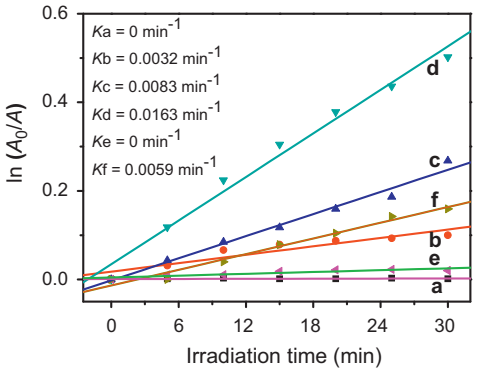

Fig. 7. Photocatalytic decomposition of MO solution by various photocatalysts: (a) Bi_2WO_6, (b–e) Ag_2O/Bi_2WO_6 composite nanoparticles calcined at (b) 100 °C, (c) 200 °C, (d) 350 °C, (e) 450 °C, and (f) $TiO_{2-x}N_x$. The inset shows their corresponding apparent rate constants (k).

show the type IV isotherm with type H3 hysteresis loop according to Brunauer–Deming–Deming–Teller (BDDT) classification [30], indicating the presence of mesopores (2–50 nm) [26,27]. Moreover, the observed hysteresis loop approaches $P/P_0 = 1$, suggesting the presence of macropores (>50 nm) [26,27]. The corresponding pore size distribution of the sample is shown in the inset of Fig. 6, which further indicating the presence of both mesopores and large pores. In view of the absence of pore structures in the single nanoparticles (30–100 nm) on the basis of SEM and TEM results, the mesopores (2–50 nm) can be related to the primary intra-aggregated pore in single Ag_2O/Bi_2WO_6 aggregate and the large pore (>50 nm) is caused by the secondary inter-aggregated pore. The textural parameters derived from the nitrogen adsorption–desorption isotherm data are summarized in Table 1. Considering a similar morphology and microstructures of the Bi_2WO_6 nanoparticles before and after modification by Ag_2O, the specific surface areas and pore volume of all the samples are in a narrow range of 5.9–7.2 m^2/g and 0.008–0.012 cm^3/g, respectively.

3.5. Photocatalytic activity

The photocatalytic performance of Ag_2O/Bi_2WO_6 nanoparticles was evaluated by photocatalytic decolorization of methyl orange (MO) aqueous solution, as shown in Fig. 7. It is clear that Bi_2WO_6 nanoparticles show no photocatalytic performance (Fig. 7a) even after coating metallic Ag nanoparticles (Fig. 7e). When the Bi_2WO_6 nanoparticles are modified by Ag_2O phase, the Ag_2O/Bi_2WO_6 composite photocatalysts show an obvious enhanced photocatalytic activity and MO is quickly decomposed with increasing irradiation time (Fig. 7b–d). Especially, when the calcination temperature is 350 °C, the obtained Ag_2O/Bi_2WO_6 shows the highest photocatalytic activity. Provided that the photocatalytic reaction follows a pseudo-first-order reaction, the rate constant (k) of the MO decomposition over Ag_2O/Bi_2WO_6 (350 °C) is estimated to be ca. 16.3×10^{-3} min^{-1}, a value larger than that of $TiO_{2-x}N_x$ (5.9×10^{-3} min^{-1}) by a factor of 2.8. In addition, further investigation indicates that the Ag_2O/Bi_2WO_6 nanoparticles (350 °C) also show high photocatalytic efficiency for the effective decomposition of a colorless phenol and p-chlorophenol solutions under visible-light irradiation (Fig. S1). By optimizing the experimental conditions for the Ag_2O, it is found that when the amount of Ag element is 11.8 at%, the obtained Ag_2O/Bi_2WO_6 nanoparticles show the highest photocatalytic activity (Fig. S2).

To further investigate the stability of Ag_2O on the surface of Bi_2WO_6 nanoparticles under visible-light irradiation, the following experiments were carried out. After one- and two-cycle decomposition of MO, the composition of the resulted Ag_2O/Bi_2WO_6

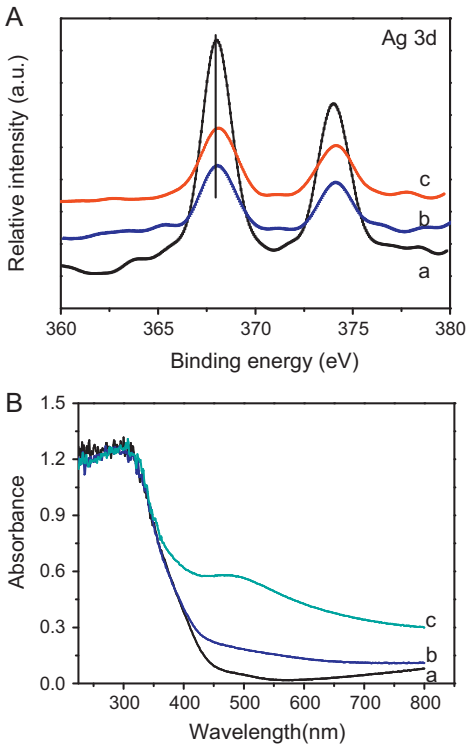

Fig. 8. (A) XPS spectra of Ag peaks: (a) as-prepared Ag_2O/Bi_2WO_6 composite nanoparticles (350 °C); (b) Ag_2O/Bi_2WO_6 composite nanoparticles after one-cycle reaction, (c) Ag_2O/Bi_2WO_6 composite nanoparticles after two-cycle reaction; (B) UV–vis spectra of (a) Bi_2WO_6; (b) Ag_2O/Bi_2WO_6 composite nanoparticles (350 °C); (c) Ag_2O/Bi_2WO_6 composite nanoparticles (350 °C) after one-cycle reaction.

nanoparticles were analyzed by XPS (Fig. 8A). Compared with the as-prepared Ag_2O/Bi_2WO_6 nanoparticles, the XPS peak of Ag shows a slight higher binding energy and a larger full width at half maximum. The slight increase of binding energy for silver element can be ascribed to the formation of particle metallic Ag due to a larger binding energy of metallic Ag [34]. To further confirm the formation of metallic Ag, the corresponding samples were analyzed by UV–vis spectra (Fig. 8B). It is clear from Fig. 8B that an new absorption at 400–600 nm is observed after visible-light irradiation, which suggests the formation of metallic Ag nanoparticles. Therefore, the Ag–Ag_2O enhance the visible-light photocatalytic activity of Bi_2WO_4 although the initial phase is pure Ag_2O. The present photostability of the Ag–Ag_2O structure is in good agreement with our recent study [35].

Bi_2WO_6 powder shows no visible-light photocatalytic activity although it can absorb visible light to ca. 450 nm according to its UV–vis spectrum in Fig. 4a. To investigate the real reason, it is important to learn the band structure of Bi_2WO_6. The CB energy level of Bi_2WO_6 can be calculated according to the equation of $E_c = -\chi + 0.5E_g$, where E_c, χ and E_g are the CB energy level, absolute electronegativity and band gap of semiconductor, respectively [36,37]. Therefore, the CB and VB energy levels of Bi_2WO_6 are calculated to be ca. +0.30 V and 3.0 V (vs. SHE), respectively. It is generally accepted that the CB level of a semiconductor should be more negative than the potential of one-electron reduction of oxygen ($O_2 + H^+ + e^- = HO_2$, −0.046 V vs. SHE) [38] in order to allow photogenerated electrons efficient transfer to oxygen. Obviously, the CB electrons of Bi_2WO_6 possess a poor reduction power owing to its more positive potential (+0.3 V, vs. SHE) than the one-electron reduction of oxygen. Therefore, the CB electrons on the Bi_2WO_6 cannot reduce oxygen effectively, resulting in negligible photocatalytic performance even after coating of metallic Ag nanoparticles (Fig. 7a and e). To further demonstrate the

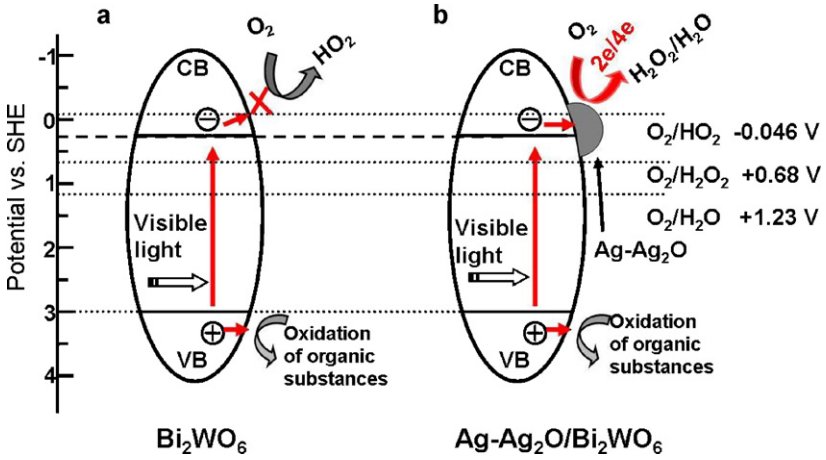

Fig. 9. Schematic diagrams illustrating the possible photocatalytic mechanism of (a) Bi_2WO_6 and (b) Ag–Ag_2O/Bi_2WO_6.

poor reduction ability of CB electrons on the Bi_2WO_6, controlled experiments were carried out as follows. When 0.46 mL of $AgNO_3$ (0.1 mol/L, Ag/Bi_2WO_6 = 10 wt%) was added into the mixing solution of Bi_2WO_6 and methyl orange, it was found that the MO could be decolorized under the identical conditions (not shown here). Considering a more positive potential of Ag^+/Ag (+0.799 V, vs. SHE) [38] than the CB of Bi_2WO_6 (+0.3 V, vs. SHE), it is believed that the CB electrons of Bi_2WO_6 are captured by Ag^+, while its VB holes remain on the VB to decompose MO. In the previous studies about the photocatalytic splitting of H_2O, a similar mechanism of Ag^+ as a sacrifice agent was widely used to promote the oxidation of H_2O by photogenerated holes in the VB of WO_3 [39,40]. After visible light irradiation for 2 h for the mixing solution of $AgNO_3$, Bi_2WO_6 and methyl orange, the obtained Ag-coated Bi_2WO_6 powder was washed with distilled water and then re-dispersed into MO solution to evaluate its photocatalytic performance. It is interesting to find that the resulted Ag-coated Bi_2WO_6 sample still shows negligible photocatalytic activity. Based on the above results, we can deduce that the low photocatalytic performance of Bi_2WO_6 and Ag/Bi_2WO_6 photocatalysts can be attributed to their poor reduction power of photogenerated electrons (Fig. 9a).

Usually, noble-metal cocatalyst (such as Ag and Au) acts as a reduction active site to promote the spatial separation of photogenerated electrons and holes, and the oxygen-reduction reaction on the noble-metal cocatalyst is expected to proceed by one-electron transfer route (O_2/HO_2, −0.046 V vs. SHE) [38]. Compared with the Bi_2WO_6 nanoparticles, in this study, it is found that the Ag–Ag_2O/Bi_2WO_6 photocatalysts show obviously higher photocatalytic activities. Therefore, it can be concluded that the CB electrons of Bi_2WO_6 can effectively transfer to oxygen by loading Ag–Ag_2O cocatalyst. In view of a more positive potential (+0.3 eV, vs. SHE) of the Bi_2WO_6 CB level compared with the one-electron reduction of oxygen (−0.046 V vs. SHE) [38], it is possible that the Ag–Ag_2O works as an electron pool and transfers the photogenerated electrons to oxygen via multi-electron transfer routes ($O_2 + 2e^- + 2H^+ = H_2O_2$ (aq), +0.682 V vs. SHE; $O_2 + 4e^- + 4H^+ = 2H_2O$ (aq), +1.23 V vs. SHE) [38] (Fig. 9b). A similar multi-electron oxygen reduction was also found on the metal-ion (such as Cu(II) and Fe(III)) grafted TiO_2 photocatalysts in our recent studies [23–25]. For the photogenerated holes, it is the organic substances that are preferable to be oxidized on the surface of Bi_2WO_6, resulting in the enhanced photocatalytic activity of Ag–Ag_2O/Bi_2WO_6 photocatalysts.

Recently, it was found that the crystalline Ag_2O particles can be used as an efficient photocatalyst for the decomposition of MO under visible-light irradiation [35]. In this study, the Ag_2O-coated Bi_2WO_6 nanoparticles also show a high photocatalytic activity. To exclude the fact that the photocatalytic activity of Ag_2O/Bi_2WO_6 nanoparticles is caused by the single Ag_2O phase, controlled experiment is performed as follows: When the Al_2O_3 was used as the precursor to prepare Ag_2O/Al_2O_3 photocatalysts; no photocatalytic activity could be detected under an identical conditions. The possible reason is that the amorphous or poor-crystalline Ag_2O phase cannot show photocatalytic activity. A similar phenomenon can be well-known for the conventional TiO_2 photocatalysts; namely, amorphous TiO_2 usually cannot show photocatalytic performance while anatase TiO_2 shows a high photocatalytic activity. However, to make this point clear, more investigation should be focused on the preparation of amorphous Ag_2O phase.

4. Conclusions

Ag_2O was demonstrated to be a new and efficient cocatalyst for the enhanced visible-light photocatalytic activity of Bi_2WO_6 nanoparticles. After the surface coating of Ag_2O cocatalyst, the obtained Ag_2O/Bi_2WO_6 composites exhibited an obvious higher photocatalytic activity than the unmodified Bi_2WO_6 nanoparticles and $TiO_{2-x}N_x$. Owing to the instability of pure Ag_2O phase, the Ag–Ag_2O is easily formed under the visible-light irradiation and work as the cocatalyst coated on the surface of Bi_2WO_6 nanoparticles. Compared with the noble-metal nanoparticle cocatalysts (such as Ag and Au) acting as the active sites for the single-electron reduction of oxygen, the Ag–Ag_2O possibly transfers photogenerated electrons to oxygen by a multi-electron transfer mechanism. This work may provide a new strategy for the design and development of high-performance visible-light photocatalysts.

Acknowledgements

This work was partially supported by the National Natural Science Foundation of China (Grants 20803055 and 20877061). This work was also financially supported by the Fundamental Research Funds for the Central Universities (Grant 2010-1a-008, 2011-1a-39, 2011-1a-16).

Appendix A. Supplementary data

Supplementary data associated with this article can be found, in the online version, at doi:10.1016/j.apcatb.2011.10.015.

References

[1] A. Fujishima, X.T. Zhang, D.A. Tryk, Surf. Sci. Rep. 63 (2008) 515–582.
[2] J.S. Chen, C.P. Chen, J.A. Liu, R. Xu, S.Z. Qiao, X.W. Lou, Chem. Commun. 47 (2011) 2631–2633.
[3] S.W. Liu, J.G. Yu, M. Jaroniec, J. Am. Chem. Soc. 132 (2010) 11914–11916.
[4] H. Yu, J. Yu, S. Liu, S. Mann, Chem. Mater. 19 (2007) 4327–4334.
[5] H. Irie, S. Miura, K. Kamiya, K. Hashimoto, Chem. Phys. Lett. 457 (2008) 202–205.
[6] F.J. Diaz, A.T. Chow, A.T. O'Geen, R.A. Dahlgren, P.K. Wong, Water Res. 43 (2009) 2750–2760.
[7] M. Ksibi, S. Rossignol, J.M. Tatibouet, C. Trapalis, Mater. Lett. 62 (2008) 4204–4206.
[8] H.G. Yu, J.G. Yu, B. Cheng, Chemosphere 66 (2007) 2050–2057.
[9] R.S. Sonawane, M.K. Dongare, J. Mol. Catal. A: Chem. 243 (2006) 68–76.
[10] I.M. Arabatzis, T. Stergiopoulos, D. Andreeva, S. Kitova, S.G. Neophytides, P. Falaras, J. Catal. 220 (2003) 127–135.
[11] J.T. Carneiro, C.C. Yang, J.A. Moma, J.A. Moulijn, G. Mul, Catal. Lett. 129 (2009) 12–19.
[12] M. Jakob, H. Levanon, P.V. Kamat, Nano Lett. 3 (2003) 353–358.
[13] J.G. Yu, J.F. Xiong, B. Cheng, S.W. Liu, Appl. Catal. B: Environ. 60 (2005) 211–221.
[14] B.F. Xin, L.Q. Jing, Z.Y. Ren, B.Q. Wang, H.G. Fu, J. Phys. Chem. B 109 (2005) 2805–2809.
[15] V. Vamathevan, R. Amal, D. Beydoun, G. Low, S. McEvoy, J. Photochem. Photobiol. A: Chem. 148 (2002) 233–245.
[16] Z.F. Liu, Z.G. Zhao, M. Miyauchi, J. Phys. Chem. C 113 (2009) 17132–17137.
[17] J. Ren, W.Z. Wang, S.M. Sun, L. Zhang, J. Chang, Appl. Catal. B: Environ. 92 (2009) 50–55.
[18] L. Amirav, A.P. Alivisatos, J. Phys. Chem. Lett. 1 (2010) 1051–1054.
[19] V. Subramanian, E. Wolf, P.V. Kamat, J. Phys. Chem. B 105 (2001) 11439–11446.
[20] N. Chandrasekharan, P.V. Kamat, J. Phys. Chem. B 104 (2000) 10851–10857.
[21] R. Abe, H. Takami, N. Murakami, B. Ohtani, J. Am. Chem. Soc. 130 (2008) 7780–7781.
[22] Z.G. Zhao, M. Miyauchi, Angew. Chem. Int. Ed. 47 (2008) 7051–7055.
[23] H. Yu, H. Irie, K. Hashimoto, J. Am. Chem. Soc. 132 (2010) 6898–6899.
[24] H. Yu, H. Irie, Y. Shimodaira, Y. Hosogi, Y. Kuroda, M. Miyauchi, K. Hashimoto, J. Phys. Chem. C 114 (2010) 16481–16487.
[25] X.Q. Qiu, M. Miyauchi, H.G. Yu, H. Irie, K. Hashimoto, J. Am. Chem. Soc. 132 (2010) 15259–15267.
[26] G.I.N. Waterhouse, G.A. Bowmaker, J.B. Metson, Phys. Chem. Chem. Phys. 3 (2001) 3838–3845.
[27] X.F. Wang, S.F. Li, H.G. Yu, J.G. Yu, J. Mol. Catal. A: Chem. 334 (2011) 52–59.
[28] H.G. Yu, J.G. Yu, B. Cheng, J. Mol. Catal. A: Chem. 253 (2006) 99–106.
[29] H.G. Yu, J.G. Yu, B. Cheng, M.H. Zhou, J. Solid State Chem. 179 (2006) 349–354.
[30] S.C. Zhang, C.A. Zhang, Y. Man, Y.F. Zhu, J. Solid State Chem. 179 (2006) 62–69.
[31] J.F. Weaver, G.B. Hoflund, Chem. Mater. 6 (1994) 1693–1699.
[32] I.M. Arabatzis, T. Stergiopoulos, M.C. Bernard, D. Labou, S.G. Neophytides, P. Falaras, Appl. Catal. B: Environ. 42 (2003) 187–201.
[33] H. He, Y. Li, X. Zhang, Y. Yu, C. Zhang, Appl. Catal. A: Gen. 375 (2010) 258–264.
[34] X.F. Wang, S.F. Li, Y.Q. Ma, H.G. Yu, J.G. Yu, J. Phys. Chem. C 115 (2011) 14648–14655.
[35] X.F. Wang, S.F. Li, H.G. Yu, J.G. Yu, S.W. Liu, Chem. Eur. J. 17 (2011) 7777–7780.
[36] Y. Xu, M.A.A. Schoonen, Am. Mineral. 85 (2000) 543–556.
[37] D.E. Scaife, Sol. Energy 25 (1980) 41–54.
[38] A.J. Bard, R. Parsons, J. Jordan, Standard Potentials in Aqueous Solution, Marcel Dekker, New York, 1985.
[39] Y. Miseki, H. Kusama, H. Sugihara, K. Sayama, J. Phys. Chem. Lett. 1 (2010) 1196–1200.
[40] A. Kudo, H. Kato, I. Tsuji, Chem. Lett. 33 (2004) 1534–1539.